Rough Surface Contact of Curved Conformal Surfaces: An Application to Rotor–Stator Rub

Philip Varney[1]
Woodruff School of Mechanical Engineering,
Georgia Institute of Technology,
Atlanta, GA 30318
e-mail: pvarney3@gatech.edu

Itzhak Green
Professor
Woodruff School of Mechanical Engineering,
Georgia Institute of Technology,
Atlanta, GA 30318
e-mail: itzhak.green@me.gatech.edu

Rotating machines and associated triboelements are ubiquitous in industrial society, playing a central role in power generation, transportation, and manufacturing. Unfortunately, these systems are susceptible to undesirable contact (i.e., rub) between the rotor and stator, which is both costly and dangerous. These adverse effects can be alleviated by properly applying accurate real-time diagnostics. The first step toward accurate diagnostics is developing rotor–stator rub models which appropriately emulate reality. Previous rotor–stator rub models disavow the contact physics by reducing the problem to a single esoteric linear contact stiffness occurring only at the point of maximum rotor radial deflection. Further, the contact stiffness is typically chosen arbitrarily, and as such provides no additional insight into the contacting surfaces. Here, a novel rotor–stator rub model is developed by treating the strongly conformal curved surfaces according to their actual nature: a collection of stochastically distributed asperities. Such an approach is advantageous in that it relies on real surface measurements to quantify the contact force rather than a heuristic choice of linear contact stiffness. Specifically, the elastoplastic Jackson–Green (JG) rough surface contact model is used to obtain the quasistatic contact force versus rotor radial deflection; differences and similarities in contact force between the linear elastic contact model (LECM) and JG model are discussed. Furthermore, the linear elastic model's point contact assumption is assessed and found to be inaccurate for systems with small clearances. Finally, to aid in computational efficiency in future rotordynamic simulation, a simple exponential curve fit is proposed to approximate the JG force–displacement relationship. [DOI: 10.1115/1.4032786]

1 Introduction

Rotor–stator rub is a common phenomenon which occurs when the rotor's deflection exceeds the allowable clearance between the rotor and stator. Eventually, such a condition results in decreased machine life via increased wear and adverse thermal effects. Detecting and preventing rotor–stator rub requires detailed knowledge of the conditions precipitating and following the onset of rub.

A necessary prerequisite for understanding, and therein diagnosing, rotor–stator rub is realistic and physically meaningful rotor–stator rub models. The first analytic rotor–stator rub investigations modeled rub by merely truncating the rotor's synchronous imbalance response [1,2]. This truncated waveform was then approximated using a Fourier series, which validated for the first time an experimentally observed rotor–stator rub phenomenon: higher harmonic shaft speed oscillations. Though enlightening as a first step, the truncation model only heuristically approximates the rotor's response, and cannot be considered a true model for rotor–stator rub.

To remedy the lack of a true rotor–stator rub model, Beatty [1] introduced the LECM. A normal restoring force is generated at the interface which is proportional to the rotor–stator interference by the contact stiffness k_c; the original work assumes a linear relationship, as do many subsequent investigations. Many authors investigating rotor–stator rub employ some variation of the LECM [3–9]. Complications to the LECM have been introduced, such as velocity-dependent friction, Hertzian contact forces [10,11], and contact damping [10,12].

Even though the LECM enjoys widespread application and demonstrates some ability to qualitatively predict the rotor response, the model is dissociated from the true nature of contacting surfaces. Estimating the contact stiffness is an inextricable complication, and a principle disadvantage of the LECM. In addition, the LECM assumes that rotor–stator rub occurs only at the point of maximum interference. However, rotor–stator rub constitutes strongly conformal contact, since the rotor–stator clearance is significantly smaller than the radii of either component; this assumption may be invalid for rotor–stator rub.

The LECM deficiencies must be addressed by considering the actual nature of the contacting surfaces. Real engineering surfaces are not smooth, but are composed of asperities of varying height (i.e., real surfaces are rough). Greenwood and Williamson [13] reduced the contact of rough elastic surfaces to that of a single composite rough surface in contact with a rigid flat, where each asperity is assumed to be hemispherical and deform elastically according to Hertzian contact. A stochastic distribution (e.g., Gaussian or exponential) is then used to describe the asperity heights, allowing the contact pressure to be found as a function of surface separation distance. However, the Greenwood–Williamson (GW) model considers only elastic deformation, and neglects the possibility of plastic deformation.

Chang et al. [14] developed the first elastoplastic rough surface contact model (the Chang–Etsion–Bogy (CEB), model). by considering a single hemispherical asperity. Beneath a prescribed critical deformation, the asperity deforms elastically according to Hertzian contact theory. Once the asperity deformation eclipses this critical value, fully plastic deformation is imposed where the asperity volume is conserved. Furthermore, each asperity is assumed to deform only near its tip. Though the CEB model provides useful conceptual understanding of elastoplastic rough surface contact, the model is not without its shortcomings. Specifically, Jackson and Green [15] show that the discontinuity at the critical deformation value leads to an overestimation of the real contact area, which in turn predicts a higher load for surfaces deforming elastoplastically than those deforming only elastically.

[1]Corresponding author.

Contributed by the Tribology Division of ASME for publication in the JOURNAL OF TRIBOLOGY. Manuscript received June 1, 2015; final manuscript received August 30, 2015; published online June 15, 2016. Assoc. Editor: Robert L. Jackson.

A closed form solution to the CEB model is provided by Green [16] where the plastic deformation is solved exactly while the elastic deformation is only approximated.

Jackson and Green [17] developed an improved elastoplastic deformation model by applying finite element methods to a single elastoplastic sphere (or asperity) contacting a rigid flat (i.e., the model considers only flattening deformation). Two important assumptions of the JG single-asperity contact model are that friction at the interface and dynamic (i.e., inertial) effects are neglected. Interestingly, Jackson and Green showed that asperity hardness is a function of both material and geometry. The results from their study were subsequently extended to rough surface contact modeling [15] (referred to henceforth as the JG model), where the model is shown to address flaws in other elastoplastic rough surface contact models (i.e., the CEB and Kogut–Etsion models) in regions of large deformations.

A novel approach for modeling rotor–stator rub is presented herein which uses rough surface contact models to approximate the contact forces generated between the rotor and stator. The objective here is not to simulate the rotordynamics, but to instead provide a method for expediently calculating the contact force given a prescribed rotor position. First, the clearance between the rotor and stator is found as a function of set-point clearance, rotor location, and circumferential position by appealing to well-known results gleaned from journal bearing mechanics. Once the clearance is known, the JG elastoplastic rough surface contact model is used to find the contact pressure at each circumferential location, from which the contact force is extracted via integration. The contact forces found using the JG model are compared to those found using both the GW and CEB models. The results are used to: (1) ascertain the influence of plasticity, (2) assess the validity of the LECM's point contact assumption, and (3) provide an important qualitative comparison to the LECM. Finally, a curve-fitting approach is suggested for approximating the quasistatic contact force as a function of rotor radial deflection.

2 System Modeling

Here, a brief summary of the system under consideration is given to familiarize the reader, although this work concerns only quantifying the quasistatic rub forces and comparing to the LECM contact forces. Consider the externally supported Jeffcott rotor shown in Fig. 1, where the support stiffness is defined in the inertial $xy\zeta$ reference frame. The inertial axis ζ extends along the length of the rotor (later, z will be used to signify asperity height). Two rotor degrees-of-freedom are selected, u_x and u_y, which are the deflection of the rotor's geometric center C, referenced from the undeflected position of the rotor O. The equations of motion including imbalance, gravity, and rub forces are

$$m\ddot{u}_x + c\dot{u}_x + ku_x = m\epsilon n^2 \cos(nt) + F_{cx} \tag{1}$$

$$m\ddot{u}_y + c\dot{u}_y + ku_y = m\epsilon n^2 \sin(nt) - mg + F_{cy} \tag{2}$$

where the rotor's constant rotational speed is n. The rotor mass is m, the external viscous damping coefficient is c, and the symmetric bearing stiffness is k. The rotor's center of mass is offset from the geometric center by the eccentricity ϵ. The rotor is constrained within a stationary housing (i.e., the stator), where the clearance is δ (this clearance is shown exaggerated in Fig. 2; in reality, the radius of the rotor is significantly greater than the clearance).

As the rotor and stator draw sufficiently close, the asperities on each rough surface interact, generating a normal contact force per unit area, $\rho(\theta, \zeta)$, where θ is defined from the inertial x axis and ζ extends along the rotor's length. Integrating the contact pressure over the contact area gives the resultant contact forces in the x and y directions

$$F_{cx} = R_r \int_0^{2\pi} \int_{-B/2}^{B/2} \rho(\theta, \zeta) \cos\theta \, d\zeta \, d\theta \tag{3}$$

$$F_{cy} = R_r \int_0^{2\pi} \int_{-B/2}^{B/2} \rho(\theta, \zeta) \sin\theta \, d\zeta \, d\theta \tag{4}$$

where R_r is the rotor radius and B is the width in the ζ direction over which contact occurs (i.e., the smaller value between the rotor and stator width). Since rotor tilting (rotation about the x and y axes) is excluded, the pressure is uniform in the ζ direction and is therefore only a function of circumferential position. In such a manner, disallowing pressure variations in the ζ direction also implicitly assumes that edge effects are negligible and that surface

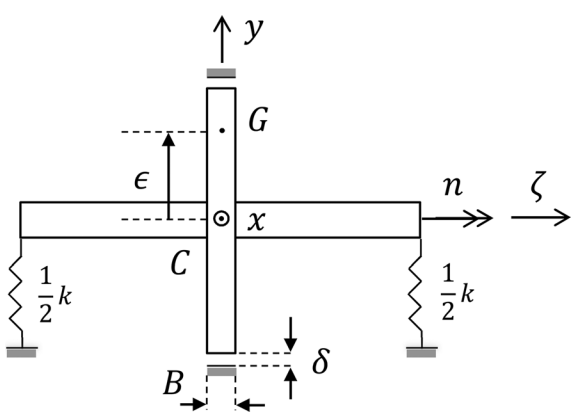

Fig. 1 Jeffcott rotor with prescribed stator set-point clearance

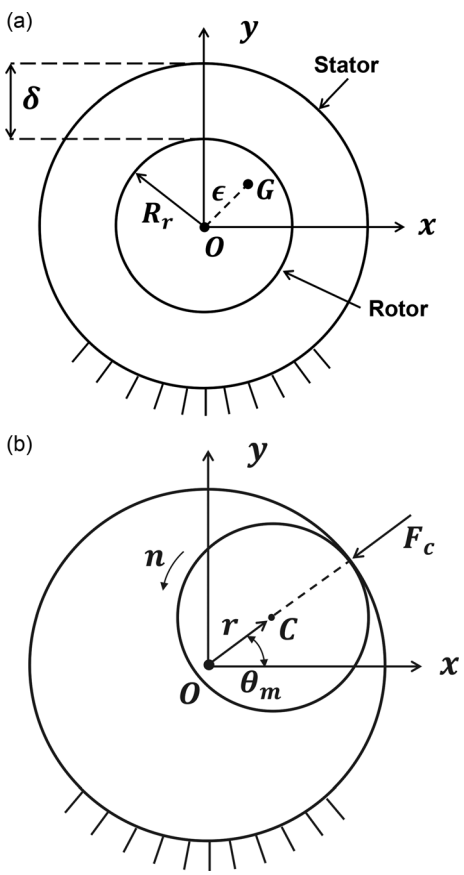

Fig. 2 Lateral contact: (*a*) Undeflected rotor–stator system and (*b*) Deflected rotor with lateral contact

roughness is uniform in the ζ direction. Thus, Eqs. (3) and (4) reduce to

$$F_{cx} = R_r B \int_0^{2\pi} \rho(\theta)\cos\theta \, d\theta \tag{5}$$

$$F_{cy} = R_r B \int_0^{2\pi} \rho(\theta)\sin\theta \, d\theta \tag{6}$$

Importantly, this work assumes that the contact pressure generated between the rotor and stator is carried only by the surface asperities on each body; such a condition may not be appropriate for severe rub between the rotor and stator. When severe rub persists, significant surface modification occurs along with bulk rotor and stator deformation; these conditions typically signify machine failure. Any successful real-time condition monitoring system should detect incipient rotor–stator rub prior to machine failure. Consequentially, the objective here is to provide improved models for detecting light rub rather than predicting severe rub-impact behavior. The JG rough surface contact model will now be used to provide the contact pressure as a function of circumferential position, surface parameters, and rotor deflection.

3 Surface Roughness Modeling

Calculating the contact force between the rotor and stator using a rough surface contact model requires several steps. First, the circumferential clearance between the rotor and stator must be found as a function of rotor degrees-of-freedom. Once the circumferential clearance is known, the average contact pressure at each circumferential location will be found using the JG rough surface contact model. Finally, the total contact force is found by integrating the contact pressure over the entire rotor surface (i.e., the nominal contact area).

3.1 Circumferential Clearance. An expression must first be developed that provides the rotor–stator clearance as a function of circumferential position and rotor displacement (see Fig. 3). Here, an expression commonly used to provide journal bearing film thickness is modified to obtain the circumferential clearance [18], where the underlying assumption is that the set-point clearance δ is much smaller than the rotor and stator radii. Consider a rotor whose deflection is $r = (u_x^2 + u_y^2)^{0.5}$, oriented from the inertial x axis by θ_m. The clearance between the rotor and stator is then a function of circumferential position, set-point clearance, and rotor displacement

$$h(\theta) = \delta[1 - (r/\delta)\cos(\theta - \theta_m)] \tag{7}$$

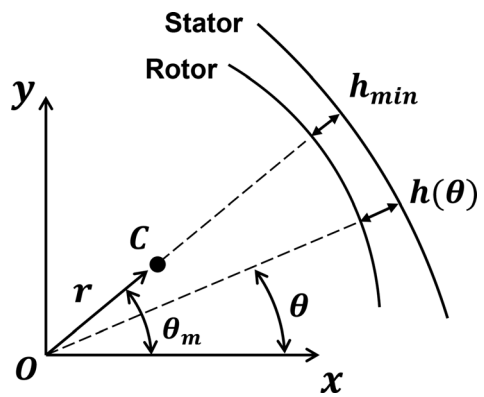

Fig. 3 Clearance between the rotor and stator as a function of circumferential position

Equation (7) provides the separation distance between the rotor and stator, which reaches its minimum value $h_{\min}$ at a circumferential location commensurate with the rotor's angular position, θ_m.

3.2 JG Rough Surface Contact Model. As the rotor–stator circumferential clearance approaches the surface roughness dimension, the asperities on each surface begin to interact, generating contact pressure between the surfaces. The contact pressure magnitude is then quantified via a particular rough surface contact model; here, the JG model will be used.

In the same manner as the elastic GW model, the contact of two opposing rough surfaces is reduced to that of one rigid flat contacting a single composite rough surface (see Fig. 4). The asperity heights z are defined from the mean asperity height, while the separation distance between the mean surface height and the contacting rigid flat at each circumferential position is the circumferential clearance $h(\theta)$. The standard deviation of surface heights and asperity heights are σ and σ_s, respectively, and are related by

$$\sigma^2 = \sigma_s^2 + \frac{3.717 \times 10^{-4}}{\eta^2 R^2} \tag{8}$$

where η is the composite areal asperity density and R is the composite average asperity radius of curvature [13]. The parameters R, σ, and η can be found from surface topography measurements using the spectral moments approach presented by McCool [19]. In addition, McCool provided a method for calculating composite surface parameters using surface topography measurements from two contacting rough surfaces. The distance between the mean surface height and the mean asperity height is y_s, as shown in Fig. 4. Here, the asperity heights are presumed to obey a Gaussian distribution $\phi(z)$

$$\phi^*(z^*) = \frac{1}{\sqrt{2\pi}}\left(\frac{\sigma}{\sigma_s}\right)\exp\left[-0.5\left(\frac{\sigma}{\sigma_s}\right)^2 (z^*)^2\right] \tag{9}$$

where the superscript $(\cdot)^*$ signifies normalization by σ_s.

Jackson and Green [15] extended a finite element study of flattening elastoplastic hemispherical contact to a rough surface contact model, where hardness is shown to be a function of both geometry and material properties (see Ref. [17] for further details). The interference between each asperity and the contacting rigid flat is $\omega = z - d$, where d is the general surface separation distance (here, $d = h(\theta) - y_s$). The critical interference ω_c at the initial point of yielding is derived from the von Mises yield criterion

$$\omega_c = \left[\frac{\pi(CS_y)}{2E'}\right]^2 R \tag{10}$$

where the product (CS_y) is calculated according to the procedure specific by Green [20]. Specifically, the method accounts for

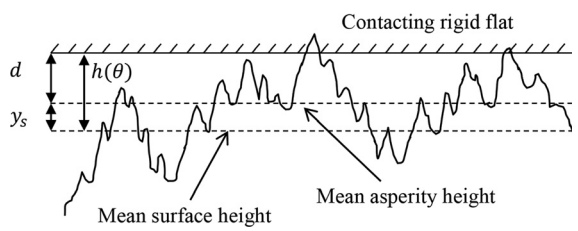

Fig. 4 Contact between two rough surfaces is reduced to that of contact between a rigid flat and a composite rough surface. Here, the surface separation distance $h(\theta)$ is shown for a single value of θ.

distinct surface material properties by calculating the product $(CS_y) = \min(C(\nu_1)S_{y1}, C(\nu_2)S_{y2})$, where the subscripts 1 and 2 refer to the respective contacting surfaces and S_y and ν are the surface yield strength and Poisson's ratio, respectively. Using the critical interference, the contact force at the point of initial yielding is

$$\bar{P}_c = \frac{4}{3}\left(\frac{R}{E'}\right)^2\left[\frac{1}{2}\pi(CS_y)\right]^3 \tag{11}$$

where the over-bar signifies a single asperity (i.e., contact between a sphere and a flat). Here, E' is the composite elastic modulus for the contacting surfaces, and is calculated according to the Hertzian procedure discussed by Greenwood and Williamson [13]. For small deformations, $0 \le \omega/\omega_c \le 1.9\omega_c$, the solution is essentially identical to the GW model. For $\omega > 1.9\omega_c$, the contact force acting on a single asperity is

$$\bar{P} = \bar{P}_c\left\{\left[\exp\left(-\frac{1}{4}\left(\frac{\omega}{\omega_c}\right)^{5/12}\right)\right]\left(\frac{\omega}{\omega_c}\right)^{3/2} + \frac{4H_G}{(CS_y)}\left[1-\exp\left(-\frac{1}{25}\left(\frac{\omega}{\omega_c}\right)^{5/9}\right)\right]\left(\frac{\omega}{\omega_c}\right)\right\} \tag{12}$$

where

$$B = 0.14\exp(23e_y) \tag{13}$$

$$e_y = \frac{S_y}{E'} \tag{14}$$

$$\frac{H_G}{S_y} = 2.84\left[1-\exp\left(-0.82\left(\sqrt{\frac{\omega}{R}}\left(\frac{\omega}{1.9\omega_c}\right)^{\frac{B}{2}}\right)^{-0.7}\right)\right] \tag{15}$$

As alluded previously, Eq. (15) indicates that surface hardness H_G depends on material properties, surface geometry, and deformation magnitudes.

Still, Eq. (13) only provides the contact force acting on a single asperity. When the rigid flat and composite rough surface are separated by a distance d, any asperity whose height exceeds d contacts the rigid flat. Thus, the contribution of all asperities of height z toward the total contact force at circumferential location θ is

$$\tilde{P}(z,\theta) = \eta A_n \bar{P}(z-d)\phi(z) \tag{16}$$

where A_n is the nominal contact area. Thus, the total contact force at a prescribed surface separation distance is found by summing the contribution of all asperities whose height exceeds the surface separation distance. Such a summation is achieved by integrating equation (16) over the entire contact range

$$P(\theta) = \eta A_n \int_d^\infty \bar{P}(z-d)\phi(z)\,dz \tag{17}$$

Since the surface separation distance $h(\theta)$ is a function of circumferential location, Eq. (17) is evaluated separately at each circumferential location. Rather than evaluating the nominal contact area A_n for each discrete circumferential area considered, Eq. (17) is redefined to calculate the average contact pressure, $\rho(\theta) = P(\theta)/A_n$

$$\rho(\theta) = \eta \int_d^\infty \bar{P}(z-d)\phi(z)\,dz \tag{18}$$

Now, Eq. (18) is substituted into Eqs. (5) and (6) and integrated numerically to obtain the contact force acting on the rotor. It is imperative to note that the rub force considered herein is quasi-static, and neglects inertial effects at the asperities. The rub force therefore only depends on the rotor's position r; thus, a curve fit approximation of the rub force versus rotor deflection can impart a significant improvement in computational expediency. Additionally, it should be noted that Eq. (13) is used for both the loading and unloading phases of contact; hysteresis effects are therefore neglected.

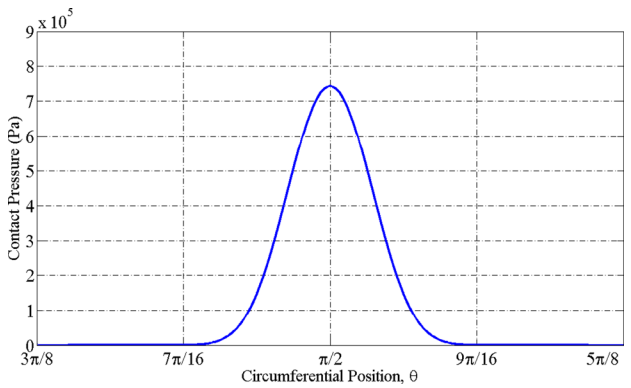

Fig. 5 Sample circumferential pressure profile obtained using rotor position $r = \delta - 3\sigma$ and $\theta_m = \pi/2$ ($\delta = 10\,\mu$m). Surface and rotor parameters are found in the Appendix, using a moderate value for plasticity ($\psi = 4.0$).

4 Results

Surface and rotor parameters used herein are provided in the Appendix, unless otherwise specified. The rough surface parameters used here are those previously measured for a real fluid film triboelement [16]. In addition, the rotor's angle of deflection is held fixed at $\theta_m = \pi/2$, with no loss of generality.

A representative circumferential pressure profile obtained by evaluating Eq. (18) is shown in Fig. 5, where the rotor's deflection is fixed to be three standard deviations of roughness from the set-point clearance (i.e., $r = \delta - 3\sigma$). The set-point clearance is taken to be $\delta = 10\,\mu$m. As expected intuitively, the maximum pressure occurs colinearly with the rotor deflection.

The relative importance of plasticity is investigated via the plasticity index ψ, defined by Greenwood and Williamson [13] to be

$$\psi = \sqrt{\frac{\sigma_s}{\omega_c}} \tag{19}$$

The plasticity index provides a measure of how likely asperities are to deform plastically; a surface with higher ψ is one in which the asperities are more likely to plastically deform. Greenwood and Williamson [13] indicated that realistic surfaces typically have plasticity indexes ranging from 0.1 to 100 (this range is considered herein). By using Eq. (10) in conjunction with Eq. (19), the plasticity index ψ can be changed by varying only the yield strength of the surface [15].

The influence of plasticity is investigated in Fig. 6 for several realistic values of the plasticity index. As expected, the contact pressure between the rotor and stator is nearly identical for surfaces whose plasticity index is very low ($\psi < 1$). In fact, the deformation in those limiting cases is nearly purely elastic, and is indistinguishable from the pressure that would be obtained if only the GW model were used. As the plasticity index is increased (or, conversely, if the yield strength is decreased), the contact pressure range uniformly decreases. Such a conclusion is expected, as higher plasticity indexes indicate that more asperities have saturated at the yield strength, and are thus incapable of supporting a greater load. Thus, it can be concluded from Fig. 6 that the effect of plasticity is non-negligible, and a realistic treatment of rotor–stator rub using rough surface contact should account for both elastic and plastic deformations.

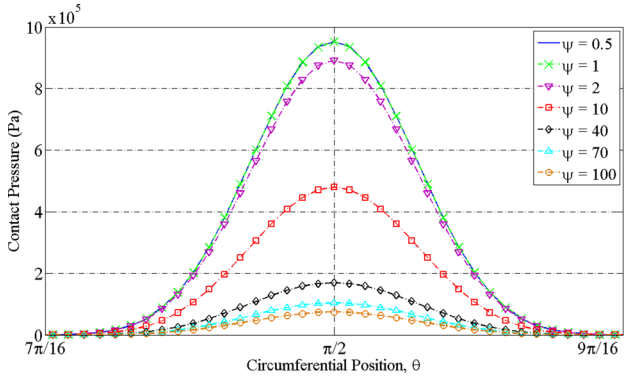

Fig. 6 Quantifying the influence of plasticity by varying the surface yield strength S_y

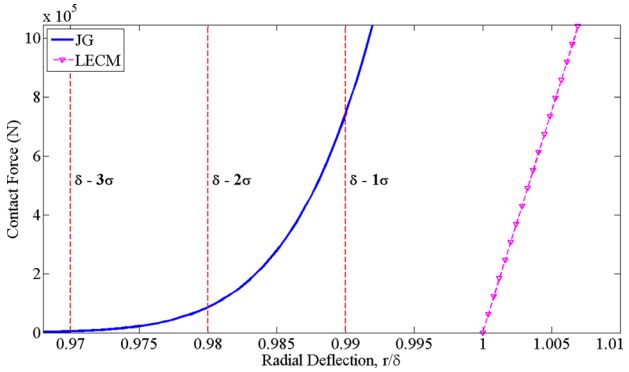

Fig. 8 Comparing the LECM and the JG rough surface contact model ($\psi = 4$, $\delta = 10\ \mu$m)

However, it is important to note that the current approach does not attempt to quantify surface damage induced from rotor–stator contact, which would occur given prolonged severe rotor–stator rub. Furthermore, the goal of a successful diagnostic system should be to detect incipient faults prior to significant component damage, precluding the necessity to quantify cumulative surface damage.

4.1 Comparing the LECM and JG Contact Models. Recall that a primary assumption of the LECM is that contact occurs only at a single point. The veracity of this assumption is investigated here by observing the circumferential contact arc as a function of set-point clearance (i.e., the influence of strongly conformal surfaces). Figure 7 provides the contact pressure for a range of set-point clearances. Note that each contact pressure profile shares the same maximum pressure in each case; this is because the minimum rotor–stator separation distance has been held fixed at $r - \delta = 3\sigma$. As the surfaces become more conformal, the contact arc likewise increases. For a set-point clearance of $10\ \mu$m, which is a realistic value in many fluid film triboelements, the contact arc extends approximately $\pi/4$ rad. Thus, for strongly conformal surfaces, the assumption of point contact in the LECM is clearly flawed.

The LECM and rough surface contact models are fundamentally different, even beyond the point contact assumption. To demonstrate qualitative differences between the rotor–stator rub models, the contact force versus rotor deflection for both models is shown in Fig. 8, using an LECM contact stiffness of $k_c = 1.5(10)^8$ N/m. The particular contact stiffness was chosen strictly for comparison aesthetics, though the need to arbitrarily select a contact stiffness certainly reinforces the LECM's primary flaw: a disassociation from the physics of contact.

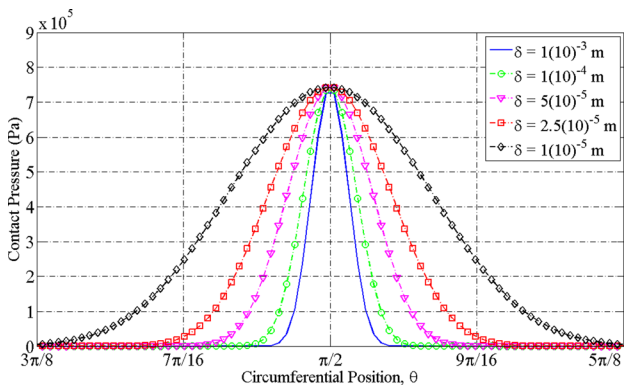

Fig. 7 Assessing the LECM's point contact assumption by varying the clearance, while holding $r = \delta - 3\sigma$ constant ($\psi = 4$)

Several qualitative observations can be drawn from Fig. 8. First, the LECM switches on immediately when the rotor's deflection r exceeds the clearance δ. On the other hand, the JG rough surface contact models predict a gradual increase in the contact force as more asperities on the rotor and stator interact. This dependence is highlighted in Fig. 8 by showing an increase in the contact force versus clearance as a function of surface height standard deviations σ. Another important difference between the force–displacement relationship using both contact models is evident. Whereas the LECM is constrained to be linear, the JG rough surface contact model predicts a nonlinear force–displacement relationship; such a distinction could likely influence the rotordynamics of the system. The differences between the LECM and JG quasistatic rotor–stator rub models are summarized below:

(1) *Force–displacement relationship*: switching (LECM) versus gradual (JG) behavior.
(2) *Force*: linear (LECM) versus nonlinear (JG).
(3) *parameter selection*: arbitrary (LECM) versus measurement-based (JG).
(4) *Contact physics*: bulk deformation (LECM) versus asperity interaction (JG).
(5) *Contact physics*: point contact (LECM) versus contact arc (JG).

Differences in switching behavior and force–displacement nonlinearity indicate that the two models are fundamentally different, both qualitatively and quantitatively. Yet, more important is that the JG rough surface contact model does not rely on any a priori choice of parameters, but is instead dictated by real and measurable surface parameters. One advantage of the LECM remains: computational expediency. This concern will be addressed in Sec. 4.2. In addition, the scale over which contact occurs is minute, and comprises only a small fraction of the rotor–stator clearance. Even though the scale may indeed be small, the differences between the models are not insignificant, as the only important scale in a system with contact is the scale over which contact occurs.

4.2 Curve Fitting the Quasistatic Contact Force. The JG rough surface contact model neglects dynamic effects at each asperity, and is therefore a quasistatic approach (as is the LECM). Thus, the contact force can be approximated using regression techniques to obtain a closed-form force–displacement relationship. This closed-form force–displacement relationship, obtained from a single simulation of rotor displacement versus contact force using the prescribed surface parameters, can then be used in a dynamic simulation of Eqs. (1) and (2) to avoid time-consuming numeric integrations required by Eqs. (5), (6), and (18).

The first step in curve fitting the contact force versus rotor deflection is to identify a suitable range of rotor deflections over which rotor rebound occurs. This range can be found by

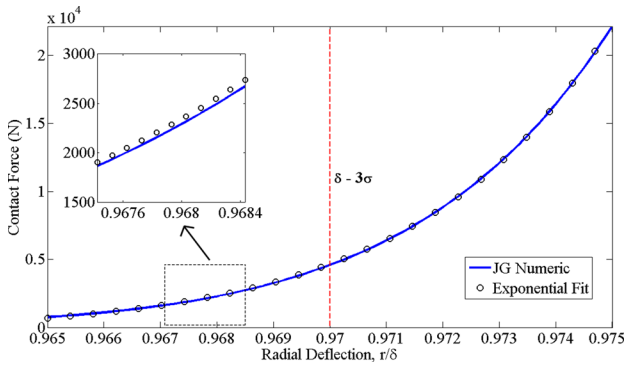

Fig. 9 Fitting the force–deflection curve using a simple exponential function ($\psi = 4$, $\delta = 10\ \mu$m)

simulating the full rotor–stator system a single time, including numeric integration of the JG model, and noting the clearance range over which rotor rebound occurs. Here, since the rotordynamics have not yet been simulated, a feasible rotor deflection range is selected and shown in Fig. 9. Note that the particular range used here is arbitrary; any similar range of rotor deflections could be cure-fit with commensurate success (though in a rotordynamic simulation, the selected range must be that over which rotor rebound occurs). After selecting the range of rotor deflections, a simple exponential fit is proposed

$$\tilde{F}_c = a_1 \exp(\lambda \tilde{r}) - a_0 \tag{20}$$

where the following normalizations have been used for numeric robustness:

$$\tilde{F}_c = F_c / \max F_c \tag{21}$$

$$\tilde{r} = \frac{r - \min(r)}{\delta \mu_r} \tag{22}$$

For the surface parameters in the Appendix and the radial range shown in Fig. 9, the coefficients are $a_0 = 0.021$, $a_1 = 0.0518$, and $\lambda = 0.876$. The radial deflection range of interest has been scaled by the clearance δ and standard deviation of the radial deflections μ_r, and shifted such that the range of interest begins at zero. It is imperative to note that the maximum and minimum values specified in the above equations pertain specifically to the radial contact range of interest. The contact force F_c is normalized by the maximum force obtained in the interval of interest. The force–displacement curve found via full numeric integration is compared to that given by Eq. (20) in Fig. 9. For the particular parameters considered here, the mean error in the approximation is 1.5%. The force–displacement relationship given in Eq. (20) is also valid only for the surface parameters given in the Appendix. Other sets of surface parameters would generate quantitatively different coefficients.

5 Conclusion

Accurate diagnostics are predicated on accurate system models; an important facet of accurate system modeling is accurately portraying each fault under consideration. Here, an improved model has been presented for one rotordynamic fault in particular: rotor–stator rub. Previously, the state-of-the-art in rotor–stator rub modeling consisted of the LECM. The LECM switches on immediately once the rotor exceeds the prescribed clearance, and thenceforth increases linearly according to the stiffness coefficient k_c. Though useful as a first step toward understanding such systems, the LECM suffers from one primary disadvantage: the arbitrary choice of the stiffness coefficient. This deficiency is addressed herein by appealing to the actual physics of contact, which for real engineering surfaces consists of asperity interaction.

A new contact model is developed using the JG elastoplastic rough surface contact model (JG), where hardness is a function of both material and surface parameters. Importantly, this new approach quantifies the contact force using real and measurable surface parameters, thus avoiding the heuristic estimation of the linear contact stiffness. The quasistatic contact force for both models is calculated and compared for relevant surface parameters, and the results indicate several differences. The JG model predicts a contact force which increases even before the set-point clearance is reached, as more asperities on the contacting surfaces interact. Furthermore, the JG model shows that the force–displacement relationship is fundamentally nonlinear.

This new formulation provides advantages even beyond more accurately quantifying the contact force. First, the new model can be used to predict contact phenomena in fluid film triboelements, since the positive finite clearances ensured by the rough surface contact model allow the fluid film forces to be easily calculated. Second, since the model relies on real surface parameters, it may be possible to re-engineer the contacting surfaces to mitigate adverse effects of rub and to prolong the life of contacting surfaces. However, the rotordynamics of such a system must be simulated prior to realizing these advantages.

Nomenclature

A_n = nominal contact area
B = rotor length
E' = composite elastic modulus
F_c = normal contact force
H_G = surface hardness
$h(\theta)$ = circumferential clearance
$\bar{P}$ = contact force on a single asperity
r = rotor radial deflection
R = average asperity radius
R_r = rotor radius
S_y = surface yield strength
u_x, u_y = rotor deflections in the x and y directions
$xy\zeta$ = inertial reference frame
z = surface heights
δ = set-point clearance
ϵ = rotor eccentricity
η = areal density of asperities
θ = circumferential position
ν = Poisson's ratio
ρ = contact pressure
σ = surface height standard deviation
σ_s = asperity height standard deviation
ψ = plasticity index
ω_c = critical interference

Appendix

The relevant surface roughness parameters are provided in Table 1. The surface parameters are those obtained by real surface measurements provided by Green [16]. The yield strength S_y is chosen by fixing the plasticity ratio ψ, according to the procedure used by Jackson and Green [15].

Table 1 Surface parameters

Parameter	Value
Equivalent modulus, E (Pa)	$25(10)^9$Pa
Surface height stand. dev., σ(m)	$1(10)^{-6}$m
Areal asperity density, η (asp/m^2)	$5(10)^{11}$asp/m^2
Asperity radius, R (m)	$2(10)^{-6}$m

Throughout this work, the rotor radius R_r and length B have been taken as 0.15 m and 0.3 m, respectively. Various set-point clearances have been investigated, as indicated where applicable.

References

[1] Beatty, R. F., 1985, "Differentiating Rotor Response Due to Radial Rubbing," J. Vib., Acoust., Stress, Reliab. Des., **107**(2), pp. 151–160.

[2] Lee, A. S., and Green, I., 1994, "Higher Harmonic Oscillations in a Non-Contacting FMR Mechanical Face Seal Test Rig," ASME J. Vib. Acoust., **116**(2), pp. 161–167.

[3] Kim, Y. B., and Noah, S. T., 1990, "Bifurcation Analysis for a Modified Jeffcott Rotor With Bearing Clearances," Nonlinear Dyn., **1**(3), pp. 221–241.

[4] Chu, F., and Zhang, Z., 1997, "Bifurcation and Chaos in a Rub-Impact Jeffcott Rotor System," J. Sound Vib., **210**(1), pp. 1–18.

[5] Sawicki, J. T., Padovan, J., and Al-Khatib, R., 1999, "The Dynamics of Rotor With Rubbing," Int. J. Rotating Mach., **5**(4), pp. 295–304.

[6] Qin, W., Chen, G., and Meng, G., 2004, "Nonlinear Responses of a Rub-Impact Overhung Rotor," Chaos, Solitons, Fractals, **19**(5), pp. 1161–1172.

[7] Zhang, W. M., and Meng, G., 2006, "Stability, Bifurcation and Chaos of a High-Speed Rub-Impact Rotor System in Mems," Sens. Actuators, **127**(1), pp. 163–178.

[8] Inayat-Hussain, J. I., 2010, "Bifurcations in the Response of a Jeffcott Rotor With Rotor-to-Stator Rub," ASME Paper No. ESDA2010-24453.

[9] Abu-Mahfouz, I., and Banerjee, A., 2013, "On the Investigation of Nonlinear Dynamics of a Rotor With Rub-Impact Using Numerical Analysis and Evolutionary Algorithms," Proc. Comput. Sci., **20**, pp. 140–147.

[10] Groll, G. V., and Ewins, D. J., 2002, "A Mechanism of Low Subharmonic Response in Rotor/Stator Contact—Measurements and Simulation," ASME J. Vib. Acoust., **124**(3), pp. 350–358.

[11] Abu-Mahfouz, I. A., 1993, "Routes to Chaos in Rotor Dynamics," Ph.D. thesis, Case Western Reserve University, Cleveland, OH.

[12] Popprath, S., and Ecker, H., 2007, "Nonlinear Dynamics of a Rotor Contacting an Elastically Suspended Stator," J. Sound Vib., **308**, pp. 767–784.

[13] Greenwood, J. A., and Williamson, J. B. P., 1966, "Contact of Nominally Flat Surfaces," Proc. R. Soc. London A, **295**(1442), pp. 300–319.

[14] Chang, W. R., Etsion, I., and Bogy, D. B., 1987, "An Elastic-Plastic Model for the Contact of Rough Surfaces," ASME J. Tribol., **109**(2), pp. 257–263.

[15] Jackson, R. L., and Green, I., 2006, "A Statistical Model of Elasto-Plastic Asperity Contact Between Rough Surfaces," Tribol. Int., **39**(9), pp. 906–914.

[16] Green, I., 2002, "A Transient Dynamic Analysis of Mechanical Seals Including Asperity Contact and Face Deformation," Tribol. Trans., **45**(3), pp. 284–293.

[17] Jackson, R. L., and Green, I., 2005, "A Finite Element Study of Elasto-Plastic Hemispherical Contact," ASME J. Tribol., **127**(2), pp. 343–354.

[18] Hamrock, B. J., 1994, *Fundamentals of Fluid Film Lubrication*, McGraw-Hill, New York.

[19] McCool, J. I., 1987, "Relating Profile Instrument Measurements to the Functional Performance of Rough Surfaces," ASME J. Tribol., **109**(2), pp. 264–270.

[20] Green, I., 2005, "Poisson Ratio Effects and Critical Values in Spherical and Cylindrical Hertzian Contact," Int. J. Appl. Mech. Eng., **10**(3), pp. 451–462.